



Seismic azimuthal anisotropy of New Zealand revealed by adjoint-state traveltome tomography



Shucheng Wu ^{a,b}, Jing Chen ^a, Ping Tong ^{a,c,*}

^a Division of Mathematical Sciences, School of Physical and Mathematical Sciences, Nanyang Technological University, Singapore, Singapore

^b State Key Laboratory of Geological Processes and Mineral Resources, China University of Geosciences, Wuhan, China

^c Earth Observatory of Singapore, Nanyang Technological University, Singapore, Singapore

ARTICLE INFO

Editor: Dr H Thybo.

Keywords:

Seismic tomography
Azimuthal anisotropy
New Zealand plate boundary
Subduction zone deformation
Adjoint-state method

ABSTRACT

The omission of seismic anisotropy in current reference models covering the entire New Zealand has been an obstacle to achieving a comprehensive understanding of deformation and dynamics along the complex Pacific-Australian plate boundary segment. Here we present a 3D azimuthally anisotropic model that encompasses both the North and South Islands of New Zealand to a depth of 40 km, using over 1 million local P-wave arrival times and a newly developed adjoint-state traveltome tomography technique. This model is built upon the New Zealand-wide 3D isotropic velocity model, serving as an essential and incremental update to the existing model. Our new model highlights significant variations in anisotropy across the plate boundary region, indicating distinct deformation states between tectonic blocks. In the North Island, pronounced along-strike changes in anisotropy are evident beneath the Hikurangi forearc, which could be attributed to variations in stress regime associated with the oblique plate convergence and changes in interseismic coupling of the subduction megathrust. The oblique plate motion further induces pure shear deformation in the middle to lower crust of the southern backarc, resulting in strong anisotropy with fast axes perpendicular to the principal axes of maximum horizontal compression. In contrast, seismic anisotropy in the central South Island primarily stems from the preferential alignment of minerals, notably within the Haast schist in the Otago block. However, anisotropy in the middle to lower crust of the northern South Island may represent inherited structures that originated during past southward subductions along the Gondwana margins at ~100 Ma. Our new model offers valuable insights into the intricate geological processes occurring within the plate boundary region.

1. Introduction

The geological basement of New Zealand primarily comprises Mesozoic terranes accreted along the southeast Gondwana margin, having undergone significant later deformation including horizontal translations, vertical axis block rotations, episodes of extension, and a series of metamorphic overprints to shape the present-day plate boundary region between the Pacific and Australian plates (Mortimer, 2004). The current plate boundary configuration of the region exhibits a high degree of diversity, changing from an oblique convergence in the North Island, to transpression in the central South Island, and to a polarity-reversed subduction of the Australian plate underneath the Pacific plate in the southern South Island beneath Fiordland (Fig. 1). Given the complex evolutionary history and structural heterogeneity of the region, constructions of high-resolution seismic models become

imperative to comprehensively unravel the plate boundary dynamics and associated deformation.

Three-dimensional (3D) variations in seismic velocity have been well-documented across New Zealand, notably with the establishment of a nationwide reference model since 2010 (Eberhart-Phillips et al., 2010, 2022). Over the years, the current version 2.3 has evolved to include 3D variations of P- and S-wave velocity as well as seismic attenuation, providing a valuable reference for studying the intricate deformation and dynamics within the plate boundary region (e.g., Reyners et al., 2011; Williams et al., 2013). However, the model currently lacks information on seismic anisotropy, which hinders in-depth analyses of the deformation states in the region. Seismic anisotropy, which refers to the directional dependence of seismic velocity within a rock matrix, serves as a powerful tool for sampling dynamic processes in the crust and mantle (Zhao et al., 2016). Previous studies on seismic anisotropy in

* Corresponding author.

E-mail address: tongping@ntu.edu.sg (P. Tong).

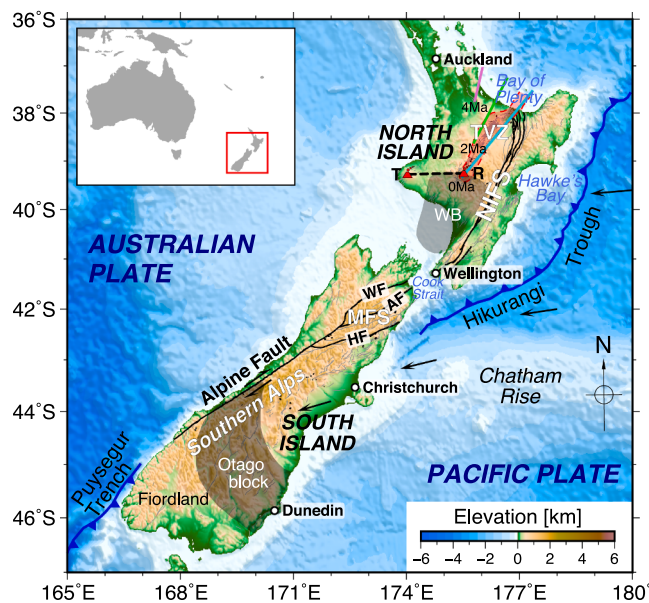


Fig. 1. Topographical map of New Zealand featuring key geological features. Active faults are represented by black and gray solid lines (sourced from GNS Science), while convergent plate boundaries are denoted by thick blue lines (Williams et al., 2013). The Taupō Volcanic Zone (TVZ) is outlined by the red-shaded region, with the adjacent color-coded lines depicting historical locations of the volcanic front from 4 million years ago to the present (Stern et al., 2006). The thick dashed line represents the ‘Taranaki-Ruapehu line’, geographically linking the Taranaki (T) and Ruapehu (R) volcanoes. The black arrows show the motion of the Pacific Plate in an Australian Plate-fixed framework. NIFS represents the North Island Fault System, with its western branch marking the boundary between the Hikurangi forearc and the backarc. Other abbreviations in the map include the Marlborough Fault System (MFS), Hope Fault (HF), Awatere Fault (AF), Wairau Fault (WF), and Whanganui Basin (WB).

New Zealand are mostly based on analyzing shear wave splitting parameters from either local or teleseismic S-waves, which suffer from a lack of resolution along depth (e.g., Balfour et al., 2005; Illsley-Kemp et al., 2019; Karalliyadha and Savage, 2013; Morley et al., 2006). Audoine et al. (2004) improved constraints on anisotropy variation in the North Island by applying a spatial averaging method to shear wave splitting data, taking into account focal depth and frequency. Meanwhile, available 3D anisotropic tomography models are only available in discrete regions in the central/eastern North Island and northeastern South Island, with plenty of room for improvement given the limited amount of data used and the spatial coverage of the models (Eberhart-Phillips and Mark Henderson, 2004; Eberhart-Phillips and Reyners, 2009; Fry et al., 2014). Therefore, there is a growing demand for a nationwide 3D anisotropic model that can be used to understand the mechanisms of varying deformation states across the New Zealand plate boundary region.

This study aims to build a 3D anisotropic model across New Zealand using local earthquake arrival times. However, this can be challenging as ray tracing in anisotropic media is numerically complex (e.g., Wang, 2014). Most previous tomographic studies have addressed this issue by employing ray paths traced in isotropic media, under the assumption that weak anisotropy does not significantly alter the paths of rays (Gou et al., 2018). Nevertheless, seismic anisotropy may have an impact similar to that of velocity heterogeneity on traveltimes observations (Zhao et al., 2016), thus neglecting anisotropy in ray tracing may introduce substantial errors to the tomographic results. In this study, we apply a new adjoint-state traveltimes tomography method (ATT) to address the issue, in which sensitivity kernels with respect to P-wave slowness (the reciprocal of velocity) and anisotropic parameters can be

precisely computed based on solving the anisotropic Eikonal equation and the transport-type adjoint equation (Tong, 2021). Therefore, no ray tracing is required in ATT, and the multipathing effect of wave propagations can be naturally captured (Tong et al., 2024). We make use of the vast amount of traveltimes data accumulated in New Zealand over the past decades, aiming to construct a high-resolution 3D azimuthally anisotropic model on top of the New Zealand-wide seismic model. The new model sheds light on how the complex plate boundary deformation is accommodated in the crust beneath the Pacific-Australian plate boundary region of New Zealand.

2. Regional tectonics

New Zealand straddles the plate boundary region between the Pacific and Australian plates, where relative plate motions vary from $\sim 60 \text{ mm yr}^{-1}$ in the northern North Island to $\sim 20 \text{ mm yr}^{-1}$ in the South Island (Wallace et al., 2004). In the North Island, plate convergence exhibits high obliquity, with margin-perpendicular motions primarily accommodated by the westward subduction of the Hikurangi Plateau, an Early Cretaceous large igneous province rifted from the Ontong Java Plateau (e.g., Barnes et al., 1998; Davy et al., 2008). The remaining margin-parallel components are absorbed by upper plate dextral strike-slip faults and clockwise rotation of the forearc, with the former slipping at a net rate of $\sim 5\text{--}20 \text{ mm yr}^{-1}$ and the latter occurring at $3^\circ\text{--}4^\circ \text{ Ma}^{-1}$ (Fig. 2a; Nicol et al., 2007).

Geodetic studies have shown that the forearc rotation is primarily driven by the southward thickening of the subducting Hikurangi Plateau (Wallace et al., 2004), characterized by an overthickened oceanic crust of $\sim 10\text{--}15 \text{ km}$ compared to a typical oceanic crust of $5\text{--}7 \text{ km}$ found further north along the Kermadec Trench (e.g., Bassett et al., 2023; Davy et al., 2008). Meanwhile, the Hikurangi margin demonstrates substantial along-strike variations in terms of megathrust slip behavior and upper plate deformation regime. In the northern segment, the plate interface beneath the forearc exhibits steady aseismic creep hosting shallow slow slip events ($< 15 \text{ km}$ depths), in stark contrast to the southern segment where deep interseismic locking persists down to a depth of $\sim 30\text{--}40 \text{ km}$ (e.g., Wallace et al., 2012a, 2004). This along-strike transition occurs at a latitude of $\sim 40^\circ\text{S}$ (see the green dashed line in Fig. 2b), and is believed to be controlled by factors such as upper plate permeability and fluid content in response to changes in effective stress in the overthrusting plate and structural heterogeneity at the slab interface (Bassett et al., 2014; Eberhart-Phillips et al., 2017; Wallace et al., 2012b). As a result of the forearc rotation, the upper plate deformation regime transitions from strike-slip/normal faulting in the north to transpressional faulting in the south, in accordance with marked changes in the maximum horizontal compressive stress ($S_{H\max}$) directions along strike (Behboudi et al., 2022; Townend et al., 2012).

The western branch of the North Island Fault System (NIFS) marks the boundary between the Hikurangi backarc and the forearc (Eberhart-Phillips and Reyners, 2009). Further west in the backarc, the Taupō Volcanic Zone (TVZ) evolves in response to the rotating forearc, with extension rates decreasing from $13\text{--}19 \text{ mm yr}^{-1}$ in the northern TVZ beneath the Bay of Plenty to $< 5 \text{ mm yr}^{-1}$ in its southern end around Mount Ruapehu (Wallace et al., 2004). The TVZ tectonically belongs to the Central Volcanic Region where high heat flux and extensive volcanic activities occur (Bibby et al., 1995). GPS and paleomagnetic data indicate that the southern hinge of the volcanic zone is gradually advancing southward into the compressional domain (the Whanganui Basin) at a rate of $\sim 10 \text{ mm yr}^{-1}$, accompanied by convective removal that progressively thins the lithosphere in the southern backarc (Stern et al., 2006). To the west of the TVZ, geodetic strain rate decreases notably, and local seismicity in the crust becomes sparse except for an earthquake cluster near Mount Taranaki (Beavan et al., 2007; Reyners et al., 2011).

In the South Island, the transition from oblique convergence to transpression occurs at the Marlborough Fault System (MFS). Here, most of the deformation is accommodated along a series of sub-parallel strike-

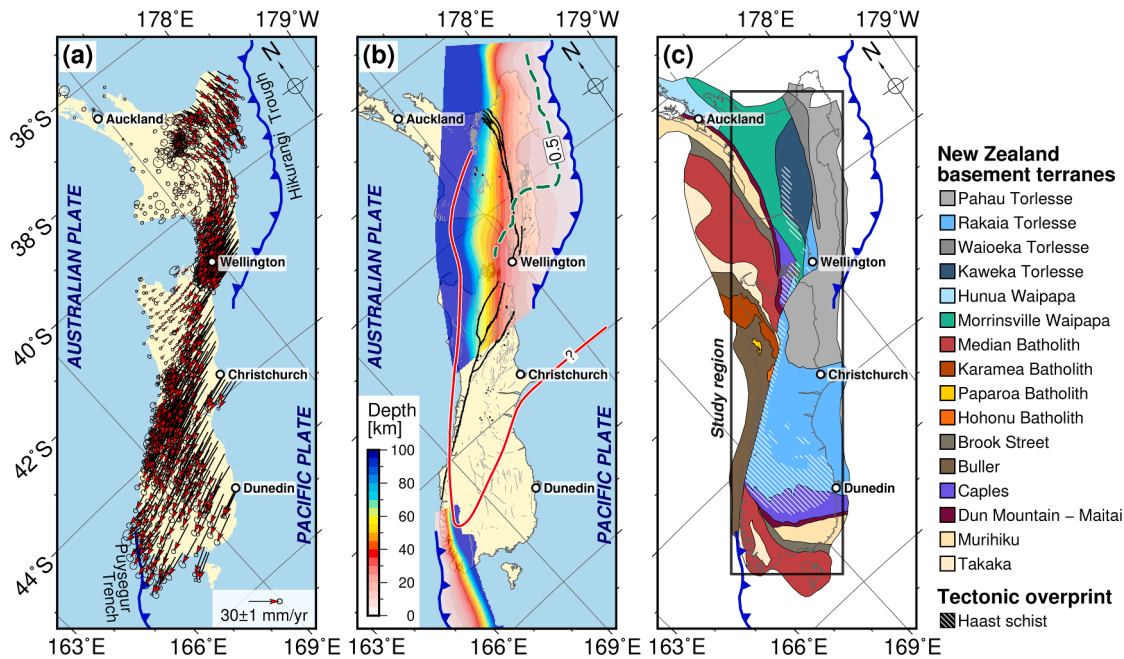


Fig. 2. Tectonic overview of New Zealand. (a) GPS velocity fields in an Australian Plate fixed reference frame (Beavan et al., 2016). (b) Depths to the upper boundary of the subducting slabs beneath New Zealand (Williams et al., 2013). Note that the thick red line denotes the possible location of the underplated Hikurangi oceanic plateau following the first episode of southward subduction along the Gondwana margin at ca. 100 Ma (Eberhart-Phillips et al., 2022; Reyners et al., 2017a). The green dashed line represents the interplate coupling coefficient of 0.5 beneath the Hikurangi margin, downdip (westward) of which the subduction megathrust is characterized by steady aseismic creep (Wallace et al., 2012a). (c) Basement terranes of New Zealand overlain by tectonic overprints of the Haast schist (modified after Mortimer, 2004). The gray rectangle defines the study region of the present study.

slip faults that align with the orientation of Pacific-Australian plate relative motion (Fig. 1). Major dextral faults constituting MFS, including the Awatere, Clarence, Wairau, and Hope Faults, generally exhibit slip rates ranging from 4 to 8 mm yr⁻¹, with the exception of the Hope Fault that slips at a much higher rate of 13–23 mm yr⁻¹ (Benson et al., 2001; Langridge and Berryman, 2005; Mason et al., 2006). The right-lateral slips on the faults within the MFS eventually transfer southward to the dominant plate-bounding Alpine Fault in the central South Island (Fig. 1). The most prominent tectonic overprints in the South Island is the Haast Schist, which represents the metamorphosed mid- to lower-crustal portion of the Jurassic-Cretaceous accretionary prism that has been rapidly exhumed and unroofed since ~135 Ma (Little et al., 1999). The schist domain spans from central Otago to the Cook Strait, tracing the eastern flank of the Alpine Fault, and includes discrete occurrences in the central North Island (Fig. 2c). Laboratory measurements and regional tomographic models have shown that the Haast schist is characterized by a uniform P-wave velocity ranging from 5.75 to 6.5 km/s and a relatively low Vp/Vs ratio of 1.5 to 1.7 throughout the crust, with very high seismic anisotropy reaching ~20 % (Eberhart-Phillips et al., 2022; Godfrey et al., 2000; Reyners et al., 2017b).

It has been suggested that the basement underlying much of the South Island likely represents the underplated portion of the Hikurangi Plateau (Fig. 2b), which has been subducted during the initial phase of southward subduction along the Gondwana margin at ~100 Ma (Reyners et al., 2011). The two-stage subduction of the oceanic plateau, characterized by nearly orthogonal directions, may have played a key role in controlling the megathrust slip behavior and defining the location of the current plate boundary (Reyners, 2013; Reyners et al., 2017a, 2017b). However, the exact geometry and spatial extent of the attached oceanic domain, particularly the southern boundary of the Hikurangi Plateau beneath the Chatham Rise and central South Island, is not well constrained mainly due to the lack of well-recorded seismicity further south and the limited resolution of seismic models for the region (Reyners et al., 2011).

3. Data and methods

In this study, we use first P-wave arrival times of local earthquakes archived in the Bulletin of the International Seismological Centre (ISC, 2022), covering the period from 1980 to 2021. Additionally, we incorporate arrival times from local earthquakes and explosive shots recorded by 47 temporary stations in the Otago Portable Network and Central Otago Seismic Array (Otago-COSA) between March 2014 and April 2015 (Eberhart-Phillips et al., 2022; Reyners et al., 2017b; Warren-Smith et al., 2017). Upon careful examination of the collected phase data, we note that ~27.3 % are associated with operator-assigned fixed focal depths (at 5 or 10 km depth), which may introduce location uncertainties potentially affecting the tomographic results. Taken together with the inherent picking errors in the ISC Bulletin, it is crucial to implement rigorous data quality control and carefully design the inversion scheme.

To ensure data quality, we apply several criteria for filtering and selecting reliable first P-wave arrivals. First, we include only earthquakes within the study domain with magnitudes greater than 1.5 and focal depths shallower than 40 km. We then discard arrivals with epicentral distances greater than 130 km. To reduce data clustering, we retain only the earthquake with the highest number of phase pickings within each 1.5 km × 1.5 km × 1.0 km block. Additionally, a linear regression analysis is performed on traveltimes to exclude outliers with biases exceeding three times the standard estimated error. Lastly, we require that each earthquake has at least 8 phase pickings and that each station records a minimum of 4 arrivals. As a result, our final dataset comprises 1058,233 first P-wave arrival times from 74,458 local earthquakes and shots, recorded by 591 stations (Figs. 3 and S1).

We apply the newly developed adjoint-state travelttime tomography (Tong, 2021) to iteratively invert for P-wave velocity and azimuthal anisotropy, starting from the 3D New Zealand-wide seismic model 2.3 (<https://zenodo.org/records/6568301>). To mitigate event location errors in the ISC catalog, we incorporate an earthquake relocation step within our three-step inversion. After the inversion, the

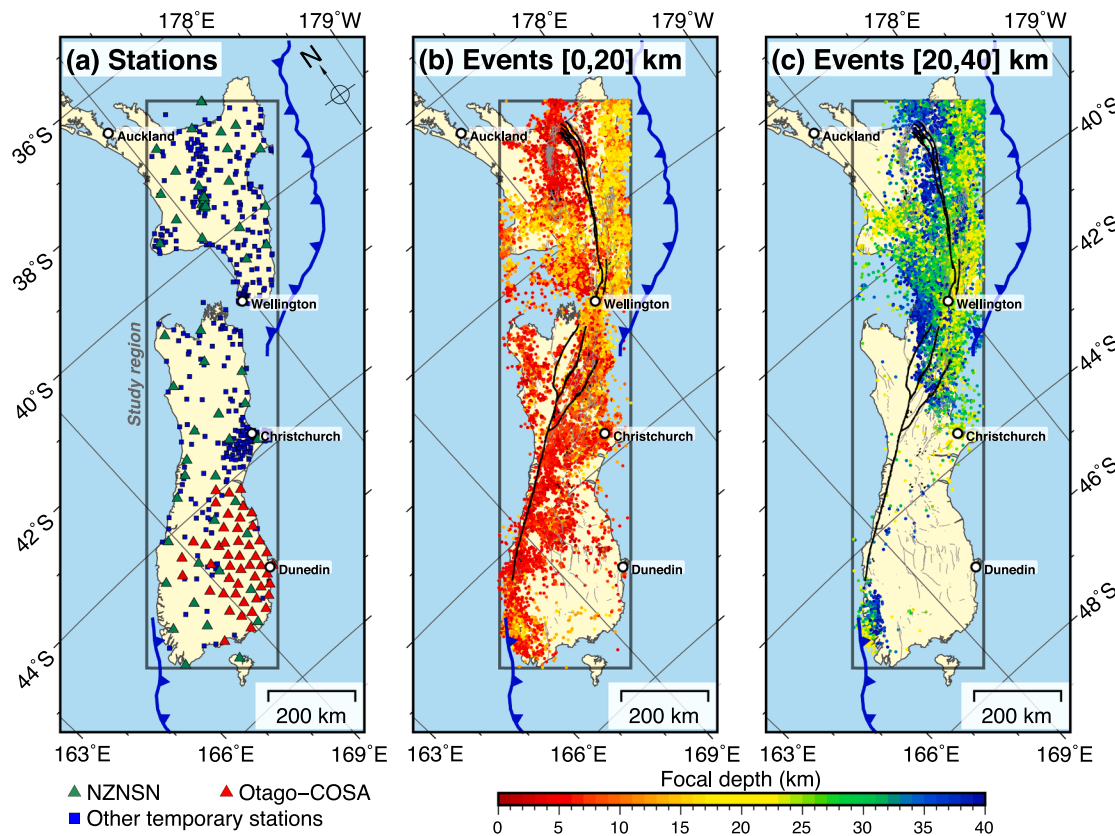


Fig. 3. Distribution of stations and local earthquakes used in this study. (a) Geographical map showing the locations of seismic stations, with different symbols representing stations from different seismic networks. NZNSN refers to the permanent New Zealand national seismic network. (b) Locations of local earthquakes with epicentral depths shallower than 20 km, color-coded by focal depths. (c) Same as (b), but for earthquakes with focal depths between 20 and 40 km.

root-mean-square traveltime residual decreases from ~ 0.78 s to ~ 0.37 s. Details of the method and inversion procedure can be found in the supporting information (Text S1).

4. Results

4.1. Resolution and uncertainty assessment

We conduct checkerboard resolution tests to assess the resolving ability of the data and the effectiveness of the tomographic inversion. The target model is defined with input anomalies characterized by a maximum perturbation of 8 % and a horizontal extent of 100 km for P-wave velocity and 150 km for azimuthal anisotropy. In the vertical direction, we set the thickness of the input anomaly to increase with depth. Note that the input anomalies are modeled as sine waves both horizontally and vertically (Fig. S2). We opt for a larger checkerboard size for anisotropy because resolving anisotropy typically demands a better data coverage compared to velocity (Huang et al., 2015). Further details regarding the resolution tests are available in the supporting information (Text S2).

Fig. 4 presents the results of the checkerboard resolution test as depth slices. It is clear that the input anomalies beneath both the North and South Island in the middle crust can be well recovered. However, at shallow depths (< 3 km), the amplitudes of the input anomaly are not fully recovered, with only about half being recovered. This could be caused by the inadequate data sampling given the subvertical ray paths at shallow depths. Nevertheless, the checkerboard pattern is generally well recovered at these depths (Fig. 4a and f). In the lower crust ($> \sim 20$ km), there are notable disparities in resolution between the North and South Islands, especially for the anisotropy (Fig. 4j). This is because most deep earthquakes occur within the subducting Pacific Plate beneath the

North Island and northeastern South Island (Fig. 3c), which makes it challenging to recover the input anomalies beneath the central and southern South Island. To investigate potential trade-offs between P-wave velocity and azimuthal anisotropy, we supplement two additional checkerboard tests with either the input velocity perturbation or anisotropy set to zero. Fig. S3 shows the results of the trade-off analyses, which indicate minor leakage (< 1 %) between velocity and anisotropy in regions with dense data coverage. Nevertheless, in fringe regions and at greater depths ($> \sim 20$ km), a slightly increased coupling between parameters becomes evident (Fig. S3e and S3j). Consequently, we primarily focus on perturbations with amplitudes exceeding 1 % in the subsequent discussion.

To further assess the robustness of our model against potential errors in the catalog, we perform four supplementary inversion tests examining event location errors and picking accuracy. The first two tests focus on event location uncertainties by excluding operator-assigned focal depths or relocating earthquakes in the starting isotropic model before tomographic inversion. The latter two tests evaluate picking accuracy by using only manually reviewed data (ISC Reviewed Bulletin) or randomly selecting 70 % of the total picks. The resulting models of the inversion tests show high consistency (Figs. S4–S7), indicating that uncertainties in the data are properly accounted for by our method and inversion scheme. Details of the inversion tests can be found in the supporting information (Supplementary Text S3).

4.2. P-wave velocity

Our final velocity model exhibits notable updates in P-wave velocity with respect to the initial New Zealand-wide seismic model. In the shallow crust, we obtain velocity increases of > 6 % beneath the central North Island and the northeastern South Island south of the Awatere

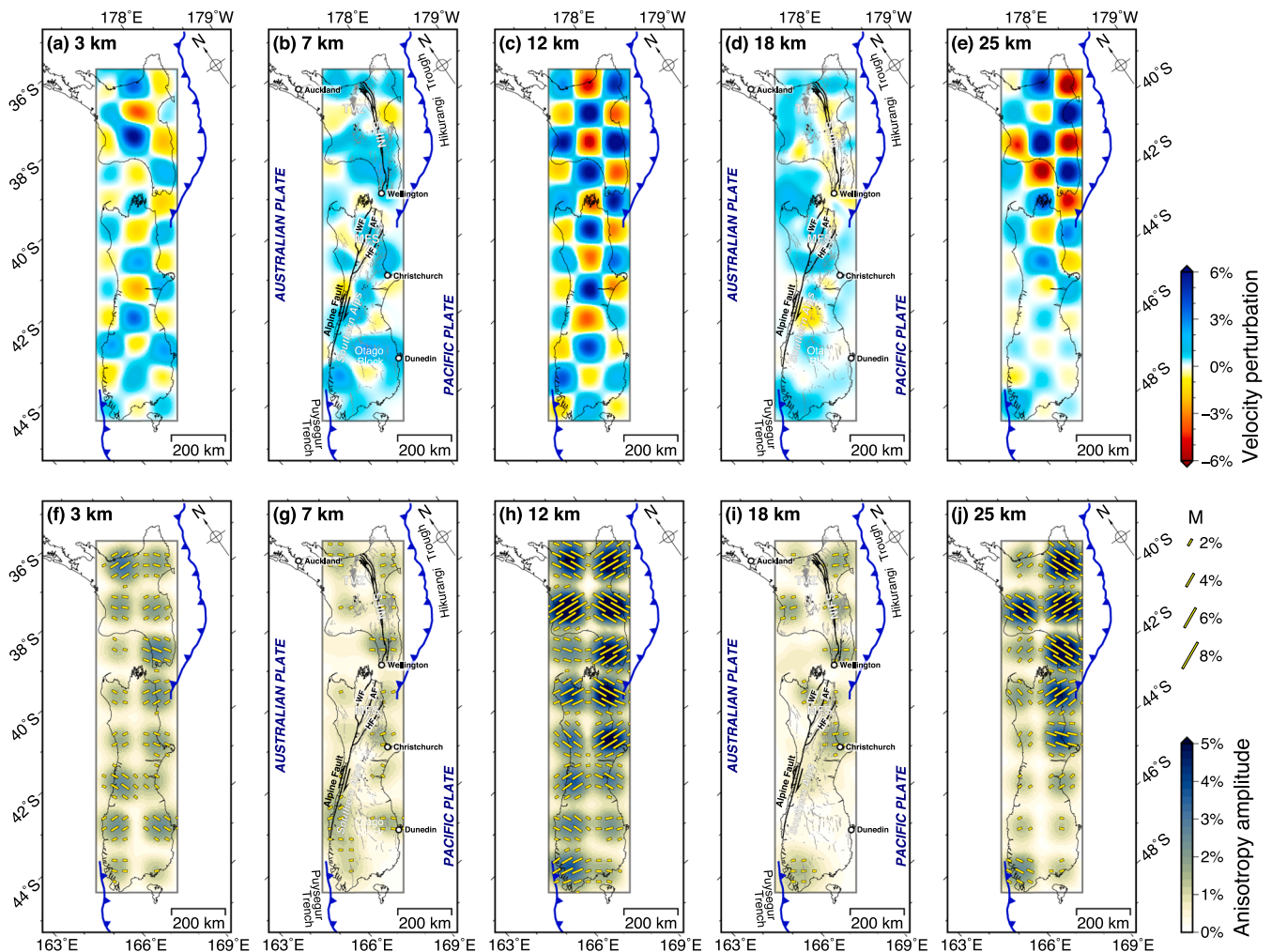


Fig. 4. Results of checkerboard resolution test shown as horizontal slices at depths of 3, 7, 12, 18, and 25 km. (a–e) Recovered P-wave velocity. (f–j) Recovered azimuthal anisotropy. The background colors indicate the amplitude of anisotropy, and the yellow bars show the direction of fast velocity axes with their lengths proportional to the amplitude of azimuthal anisotropy. Note that there are no perturbations in the input model at depths of 7 and 18 km (refer to Text S1 in the supporting information for details).

Fault (AF) (Figs. 5i and S8). Beneath the Hikurangi forearc, our model reveals velocity updates with considerable along strike variations, transitioning from relatively highs to lows from northeast to southwest, with the boundary located at a latitude of approximately 40°S (Figs. 5i and S8). Nevertheless, the low-velocity Hikurangi forearc remains a notable feature in the final model, characterized by P-wave velocities lower than 5 km/s at shallow depths (Fig. 6). In the upper crust, the TVZ is surrounded by significant high-velocity anomalies reaching up to ~6 km/s (Fig. 5e). Notably, the P-wave velocity on the western side of the TVZ is slightly higher than that on the eastern flank (Profile BB' in Fig. 6), which is highly consistent with previous controlled-source results (Stern and Benson, 2011). Beneath the central and southern South Island, velocity updates are generally minor, and the final velocity model closely resembles the initial model.

In the middle crust at ~12 km depth, we observe similar velocity updates with respect to the shallow depths beneath the forearc in the North Island. In contrast to the upper crust, the average velocity beneath the TVZ decreases slightly (Figs. 5j and S8). The decreased middle crust velocity beneath the TVZ results in a strengthened low-velocity zone, represented by a body of P-wave velocity lower than 6 km/s underlying a high-velocity lid in the upper crust (see BB' profile in Fig. 6). This feature is not obvious in the results of Stern and Benson (2011), which could be due to limited ray path coverage in the wide-angle reflection profile. However, receiver function and magnetotelluric studies indicate

low seismic velocities and high conductivities in the middle crust beneath the TVZ, suggesting regions of partial melt (Bannister et al., 2004; Heise et al., 2007). In the lower crust, our model shows an increased velocity of more than ~6 % south of the TVZ (Fig. 5k, l, and S8). This transforms the initially low-velocity lower crust (6.2 to 6.6 km/s; Fig. 5d) into an intermediate to high velocity anomaly with P-wave velocity of ~6.6 to ~7 km/s (Fig. 5h, also see CC' profile in Fig. 6). In the northeastern South Island, average velocity beneath the Marlborough Fault System (MFS) and north of Christchurch drops about 4 % with respect to the initial model (Fig. 5k and l). Overall, while our model introduces certain modifications to the P-wave velocity, it broadly retains the dominant features presented in the initial model.

We further compare our modeled P-wave velocity with the New Zealand Adjoint Tomography model (NZATOM) of Chow et al. (2022), presented as horizontal slices at selected depths in Fig. 7. Due to differences in model coverage, the comparison is focused on velocity structures beneath the North Island and the northeastern South Island. As shown in Fig. 7, while our model seems to reveal more details compared to the Vp in the NZATOM, the major velocity anomalies show broad consistency between the two models. Interestingly, we observe greater alignment in the geometry of velocity anomalies between our model and the Vs component in the NZATOM. This is possibly because the NZATOM model was constructed using low-frequency waveform data, which predominantly contains surface waves rather than direct

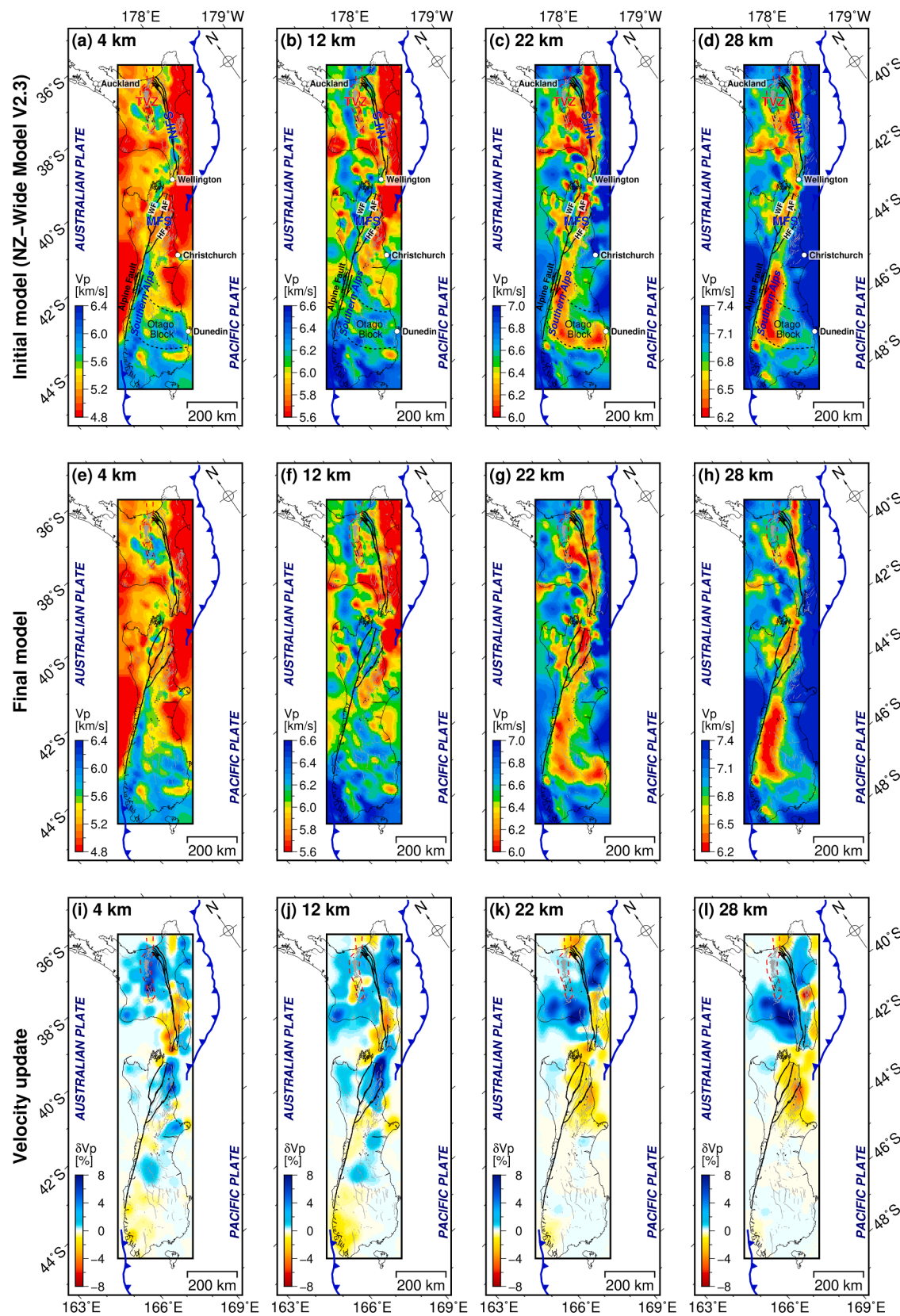


Fig. 5. Depth slices of P-wave velocity for the initial model (a–d), our final model (e–h), and velocity updates shown as perturbations (i–l) at example depths of 4, 12, 22, and 28 km.

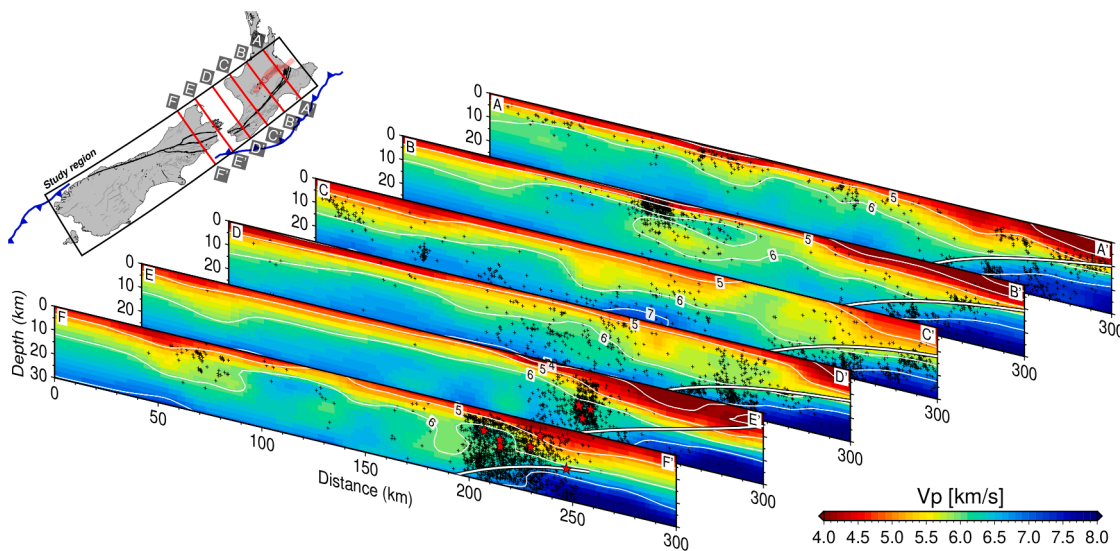


Fig. 6. Vertical transects of P-wave velocity for the final model, with locations indicated on the inset map as red lines. Black crosses and red stars represent local earthquakes with magnitudes below and above 5.5, respectively. The thick white lines depict the slab interface as per Williams et al. (2013).

waves, resulting in higher sensitivity to Vs (Chow et al., 2022). Given that most of the velocity features are well discussed in previous studies, we will mainly focus on azimuthal anisotropy in the following discussion.

4.3. Azimuthal anisotropy

We present the fast velocity directions (FVDs) and the anisotropy magnitude as depth slices in Fig. 8. Our model highlights pronounced variations in azimuthal anisotropy among different basement terranes and tectonic units of New Zealand. In the upper crust, the eastern flank of the Taupo Volcanic Zone (TVZ) stands out as a structural hinge zone in the North Island, marking a transition in anisotropy patterns (Fig. 8a and b). Beneath the backarc region in the west, the FVDs are mostly oriented north-south (N-S) and northwest-southeast (NW-SE), while the forearc exhibits significant along-strike variations in FVDs, transitioning from northeast-southwest (NE-SW) to east-west (E-W) from north to south (Fig. 8a and b). Beneath the South Island, our model primarily exhibits N-S oriented FVDs, with the exception of a NW-SE oriented FVD near Christchurch (Fig. 8a). The magnitude of anisotropy appears to increase towards the Otago block in the central South Island (Fig. 8b), although the checkerboard tests reveal an underestimated magnitude beneath most of the South Island.

In the middle crust, our model reveals more pronounced variations of azimuthal anisotropy across New Zealand (Fig. 8c and d). The along-strike transition of anisotropy beneath the Hikurangi forearc persists but the FVDs have changed significantly with respect to the shallow crust. In the northeastern forearc, our model shows NW-SE orientated fast axes that are roughly perpendicular to the trench, while the southwestern part shows more trench-parallel fast directions. The transition in FVDs along strike occurs at a similar location as in the shallow crust, roughly at latitude 40°S. Further inland, FVDs change to NE-SW beneath the North Island Fault System (NIFS) and regions east of the TVZ, gradually rotating to NW-SE towards the northernmost part of our study domain. Meanwhile, the eastern TVZ also serves as a structural boundary with sharp contrasts in seismic anisotropy (Fig. 8c). Beneath the South Island, the anisotropy pattern shows fewer variations compared to the North Island. In the central South Island, the FVDs are generally consistent with that observed in the shallow crust. However, significant contrasts in the fast directions are observed in the northeastern South Island between the two sides of the Awatere Fault (AF) in the Marlborough Fault System (MFS). To the southeast of the AF, there is

a pronounced anisotropy trending NW-SE, whereas on the northwestern side, the fast direction is oriented NE-SW. In addition, anisotropy beneath Christchurch also exhibits a different fast direction compared to the shallow crust, with an orientation of roughly N-S in the middle crust (Fig. 8c).

The patterns of azimuthal anisotropy in the lower crust exhibits similar features to those in the middle crust, with the highest magnitude located to the south of TVZ (Fig. 8e–g). The strong anisotropy is characterized by a N-S fast axis and coincides with regions with positive velocity updates (Fig. 5k). In the northeastern South Island, the AF continues as a structural boundary separating distinct anisotropy patterns, with an increased magnitude on its southeastern side compared to the middle crust (Fig. 8e–h). Note that the magnitude of anisotropy decreases with increasing depth in the central and southern South Island, reflecting the decreased resolution of our model in the specific region.

5. Discussion

5.1. Spatial variation of anisotropy along the Hikurangi margin in the North Island

5.1.1. Hikurangi forearc

Our final model shows substantial along-strike changes in fast velocity directions (FVDs) beneath the Hikurangi forearc. In the upper crust, prevalent trench-parallel (NE-SW) FVDs are evident in the northeastern segment of the forearc (Fig. 8a and b). This feature is generally consistent with local shear wave splitting analyses conducted at onshore stations, as reported by Zal et al. (2020) (Fig. S9a). By contrast, roughly plate motion-parallel (E-W) FVDs are observed in the southwestern forearc (Fig. 8a and b). As depth increases (> 8 km), FVDs beneath both segments undergo a polarity shift, transitioning from trench-normal (NW-SE) in the northeast to trench-parallel (NE-SW) in the southwest (Fig. 8c). The anisotropy transition boundary throughout the forearc crust remains positioned south of Hawke's Bay at latitude ~40°S (Fig. 8). Such along-strike variations in anisotropy and the layered structures are not present in the tomographic model of Eberhart-Phillips and Reyners (2009). Their model depicts heterogenous anisotropy with varying FVDs in the forearc, interpreted to reflect structural variations within the forearc crust (Eberhart-Phillips and Reyners, 2009). However, local shear wave splitting measurements reveal mostly NE-SW fast directions likely influenced by tectonic stress

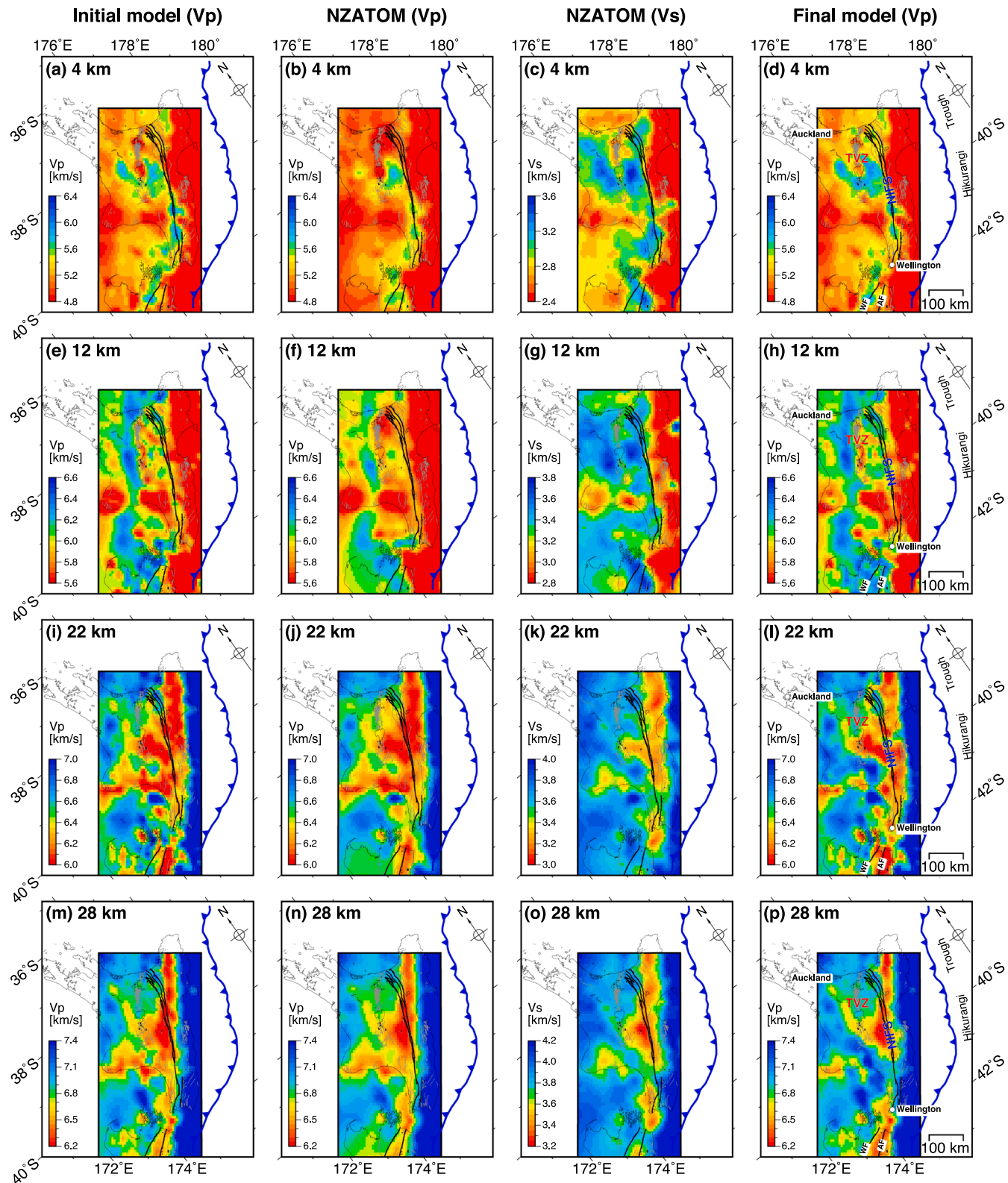


Fig. 7. Comparison of P-wave velocity at selected depths between the initial model (first column), NZATOM model (Chow et al., 2022; second and third columns), and our final model (the last column).

(Illsley-Kemp et al., 2019). Therefore, we proceed to examine the along-strike variations of anisotropy in our model concerning structure and regional stress along the Hikurangi forearc.

Azimuthal anisotropy in the upper crust is primarily controlled by the preferential alignments of microcracks, which can form due to

faulting, respond to regional stress, or result from a combination of both mechanisms (Bones and Zoback, 2006). In the Hikurangi forearc, major faults that comprise the North Island Fault System (NIFS) trend northeast, gradually bending to a more northerly strike beneath the Bay of Plenty offshore in the north (Fig. 1). In the southwestern forearc, we find

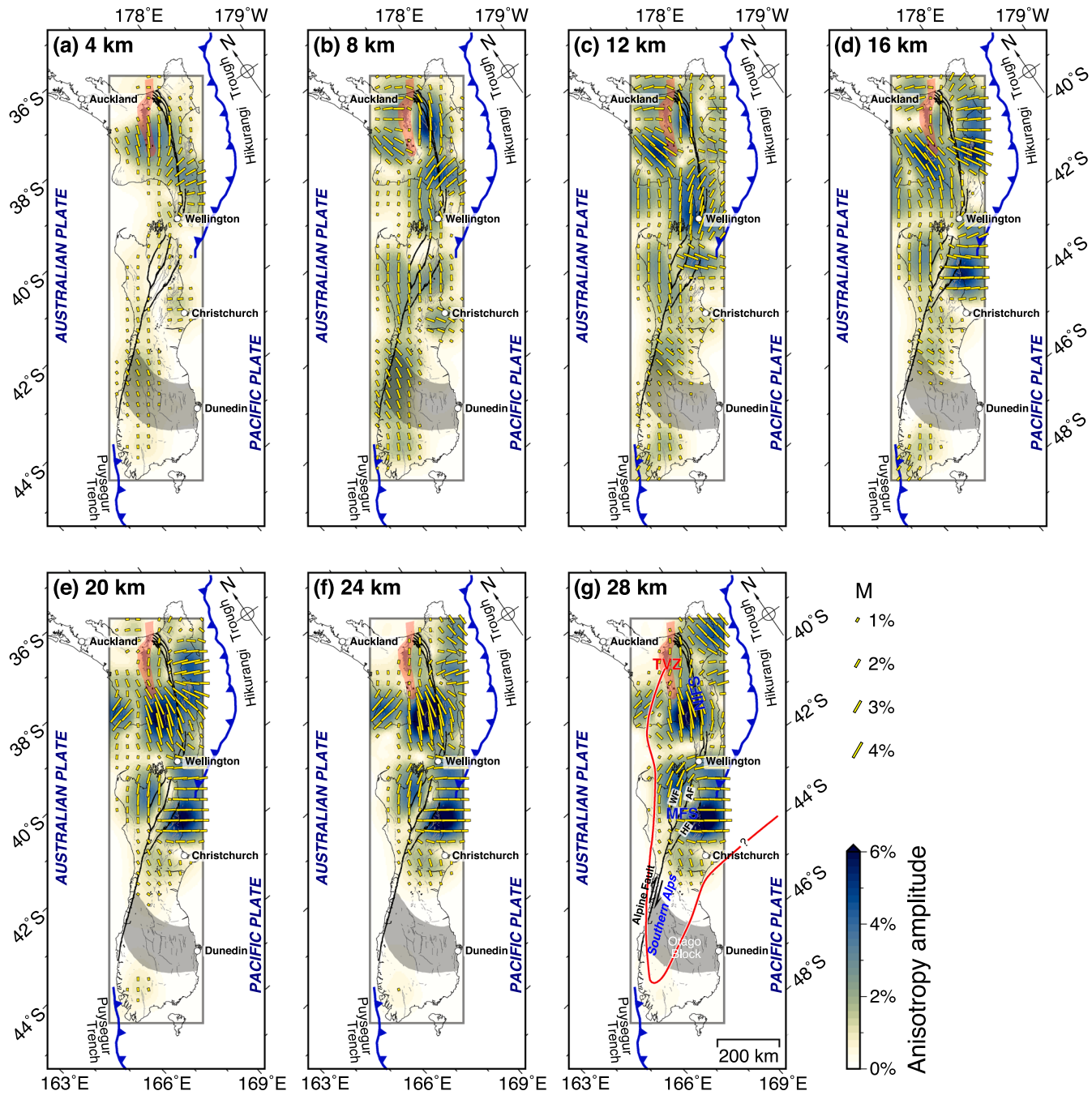


Fig. 8. Distribution of azimuthal anisotropy at seven example depths. The background colors represent the magnitude of anisotropy, and the yellow bars indicate the fast velocity direction. Symbols and abbreviations representing major geologic features on the map are consistent with those in Fig. 1.

no obvious correlation between the shallow anisotropy and fault strike (Fig. 8a), implying that structural fabrics related to crustal faulting might not be the primary cause for the observed anisotropy there. However, in the northeastern forearc, the NE-SW FVDs appear to align with the strike of the NIFS, particularly in the north approaching the Bay of Plenty where a rotation of FVDs to N-S is observed in tandem with the changes in the NIFS strike (Fig. 8b). This could suggest an increased influence of faulting on the observed anisotropy in the northern segments of NIFS. Nonetheless, a 10–20° difference between the FVDs and NIFS strike is observed west to the Hawke's Bay region near the mapped fault trace (Fig. 8b), indicating that there must be other factors governing the shallow anisotropy in the region.

We further compare the maximum horizontal compressive stress ($S_{H\max}$) orientations with the anisotropy in the upper crust, which

reveals a high level of consistency between the two observations (Figs. 9a, b, and S10). Prevailing regional stress can cause preferential opening or closure of microcracks, resulting in seismic anisotropy with FVDs parallel to the $S_{H\max}$ orientation (Boness and Zoback, 2004, 2006; Crampin, 1987, 1991). Regional stress in the forearc shows notable along-strike transitions, with $S_{H\max}$ striking NE-SW in the north to WNW-ESE in the south across the southern Hawke's Bay (Fig. 9a), which have been proposed to stem from the oblique plate convergence and the rotation of the forearc (e.g., Behboudi et al., 2022; Nicol et al., 2007; Townend et al., 2012; Wallace et al., 2004). Such transition in stress orientation precisely matches the change in FVDs along strike. We note that the observed FVDs are notably more consistent with $S_{H\max}$ measured from borehole breakouts than those derived from focal mechanisms (Fig. 9a and b). This is expected since borehole breakout

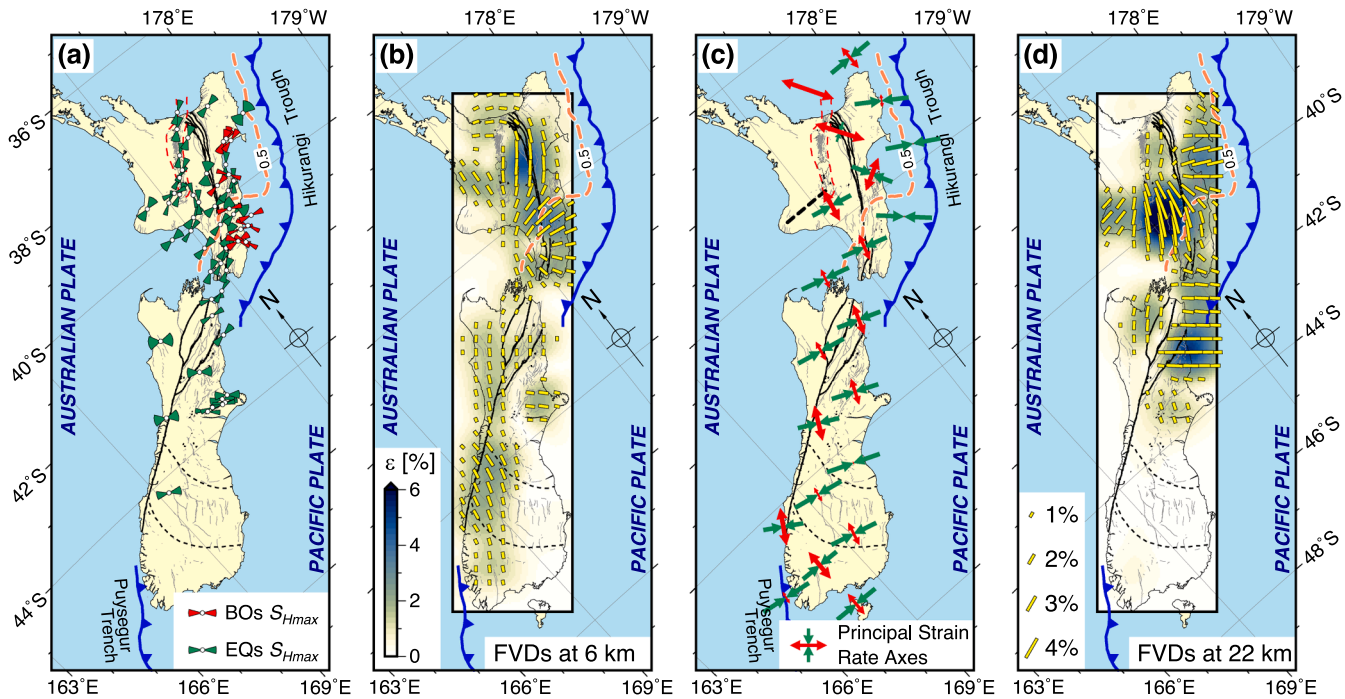


Fig. 9. Comparisons between regional stress, geodetic strain rate, and azimuthal anisotropy at different depths. (a) Maximum horizontal compressive stress ($S_{H\max}$) orientations. The “BOs” and “EQs” $S_{H\max}$ refer to the $S_{H\max}$ measured from borehole breakouts (Behboudi et al., 2022) and focal mechanism inversions (Townend et al., 2012), respectively. Note that we only include EQs $S_{H\max}$ estimated from earthquakes shallower than 50 km in the Figure. (b) Azimuthal anisotropy at 6 km depth. (c) Average principal strain rate axes (Kreemer et al., 2014). The principal strain rate axes are normalized to the maximum absolute value at each location. (d) Azimuthal anisotropy at 22 km depth. Other symbols are the same as those in Fig. 1.

measurements directly sample shallow stress (less than a few kilometers), in comparison to the focal mechanisms that generally constrain tectonic stress at seismogenic depths (Behboudi et al., 2022; Evanzia et al., 2017; Townend et al., 2012). Although the FVDs in the northern forearc generally mimic the trend of the mapped faults, they seem to be more consistent with the $S_{H\max}$ directions, particularly in regions west to the Hawke's Bay where a mismatch between the FVDs and the fault strike is seen (Fig. 9b). Therefore, we conclude that tectonic stress predominantly governs the anisotropy along the Hikurangi forearc, except for the northern segment of NIFS where structural fabrics might exert a more influential role. The transition of FVDs in the southern Hawker's Bay area thus signifies changes in the upper plate deformation regime from strike-slip/normal in the north to transpression/reverse in the south (Behboudi et al., 2022; Fagereng and Ellis, 2009; Wallace et al., 2012c).

The subducting Hikurangi Plateau beneath the forearc seats at depths of 10–30 km (Williams et al., 2013), where the north-south difference in FVDs persist but with significant polarity shifts compared to the upper crust (Fig. 8). To explain the along-strike changes in anisotropy at these depths, one possibility is that the different anisotropies represent different rock units near the subduction interface, i.e., thicker subducted and underplated sediments capping the subducting plate in the southern forearc versus thinner sediments and thus exposed oceanic crust in the north (Eberhart-Phillips and Reyners, 2012; Reyners et al., 2017a). However, the continuation of similar anisotropy pattern with increasing depths to over 20 km precludes the proposed scenario. Relationships between seismic anisotropy and megathrust slip behavior have been identified in other subduction zones such as the northeast Japan and northern Chile (Huang et al., 2019; Liu and Zhao, 2017). These studies show trench-parallel FVDs in regions where the slab interface is strongly locked, reflecting horizontal compressions along the interface. Conversely, in regions where the slab interface undergoes steady aseismic creep, stable shear deformation at the interface generates FVDs aligned with the subduction direction (Huang and Zhao, 2019).

2021). This could be the case in the Hikurangi subduction zone where the observed FVDs exhibit a strong correlation with the along-strike changes in the megathrust slip behavior (Fig. 9d).

The two-layered anisotropy discussed above might offer further insights into the previously proposed stress layering beneath the Hikurangi forearc. Mechanical decoupling between the subducting plate and the overriding plate has been invoked to account for the discrepancies between the shallow stresses and those at greater depths (Behboudi et al., 2022). Our findings in the forearc appear to support such decoupling. If the along-depth variations in anisotropy are controlled by tectonic stress, the proposed mechanical decoupling would have occurred at depths around 8–12 km where the rotations of FVDs are evident (Fig. 8). Moreover, the two-layered structure could also potentially explain the divergence between the FVDs in our model and those measured from local shear wave splitting, considering that the splitting analyses use local earthquakes down to 40 km depths beneath the forearc (Illsley-Kemp et al., 2019).

5.1.2. Hikurangi backarc

The anisotropy within the Hikurangi backarc notably differs from that observed in the forearc (Fig. 8). Transitioning in FVDs occurs between the eastern flank of TVZ and the NIFS, which aligns closely with earlier studies (Audoine et al., 2004; Eberhart-Phillips and Reyners, 2009; Morley et al., 2006). Fracturing along the margins of TVZ and the presence of mineral-induced anisotropy in the schists have been suggested as contributing factors to the margin-parallel (NE-SW) FVDs (Eberhart-Phillips and Reyners, 2009), a proposition we largely concur. Within the TVZ, despite the resolution of our model is limited, we discern rift-parallel FVDs in the center and rift-perpendicular FVDs in the northern TVZ (Fig. 8a–c). These observations are consistent with previous smaller-scale studies (Audoine et al., 2004; Eberhart-Phillips and Reyners, 2009; Illsley-Kemp et al., 2019; Johnson et al., 2011). Further west in the backarc, the prevailing upper crust anisotropy with N-S FVDs east of Taranaki (Fig. 8a and b) is likely controlled by crustal

structures. Specifically, N-S trending structures such as the Taranaki Fault and basement terranes, including Maitai, Murihiku, and Morrinsville (Fig. 2c; Mortimer, 2004), could have played a significant role in shaping the observed anisotropy. The increasing impact of structural elements on anisotropy may be associated with the reduction in geodetic strain rates in these regions (Beavan et al., 2007).

Our model shows a predominant anisotropy (amplitude > 6 %) with N-S to NNE-SSW FVDs in the middle to lower crust south of the TVZ (Fig. 8e–g), spatially correlating the notable increase in P-wave velocities (Fig. 5k). We find that the northern boundary of the anomaly roughly matches the previously defined ‘Taranaki-Ruapehu line (TR-line)’, south of which the backarc crust is ~10 km thicker than the north (Salmon et al., 2013, 2011). The TR-line also coincides changes in backarc deformation from extension in the north to shortening in the south (Stern et al., 2006), which has been proposed to play a role in controlling the along-strike variation in the interseismic coupling of the subduction megathrust (Wallace et al., 2012c). Given the abrupt changes in crustal thickness and deformation patterns across the TR-line, the presence of structural heterogeneity and anisotropy is not surprising. We compare the FVDs in the lower crust with geodetic strain rates in Figs. 9 and S10, showing great consistencies between the FVDs and the principal axes of maximum horizontal extension in the southern backarc. The presence of this feature, along with the notably increased velocities, indicate that the middle to lower crust south of the TVZ may correspond to a region with strong strain localization, inducing pure shear deformation in the ductile middle/lower crust. High Qp values (low attenuations) observed in the attenuation tomography of Eberhart-Phillips et al. (2008) may provide further evidence for the proposed strain accumulation beneath the southern backarc.

5.2. Anisotropy in the South Island

5.2.1. Central South Island

The South Island of New Zealand displays more homogeneous anisotropies compared to the North Island, partly due to limitations in data coverage (Fig. 3). In the central South Island, a predominant portion of the anisotropy hosts an N-S fast direction, with an increasing amplitude towards the Otago block where a major tectonic overprint of the Haast schist outcrops (Fig. 8a–c). Note that the actual anisotropy may have much higher amplitudes, as indicated by the underestimated anisotropy magnitudes in the checkerboard tests (Fig. 4). The observed anisotropies in the central South Island show no clear correlations with either the strike of the Alpine Fault or the orientation of stress (Fig. 9), implying that neither crustal faulting nor regional stress might be the dominate control for the observed anisotropy. It has been suggested that foliations in schist packages could be a significant contributing factor to the observed anisotropy in New Zealand (Eberhart-Phillips and Reyners, 2009; Karalliyadda and Savage, 2013). Meanwhile, anisotropy induced by crystallographic preferred orientation (CPO) of minerals within the Haast schist is strong, with amplitude exceeding 20 % as measured by laboratory experiments (Godfrey et al., 2000). Such strong mineral-induced anisotropies in schist may overprint stress-induced anisotropies that are generally with amplitudes ranging from 3 % to 10 % in the upper crust (Boness and Zoback, 2006). Meanwhile, anisotropy induced by fracturing in the fault damage zone typically remains localized within a few kilometers away from the fault trace (Audet, 2015), which is not easy to be captured by our inversion considering the data distribution. Therefore, we speculate that the observed anisotropy in the central South Island is mainly caused by CPO of minerals within the schist terranes, and the N-S FVDs may represent mineral fabrics formed during the rapid exhumation of the schistose rocks.

Geodynamic modellings incorporating rheology suggest that the Otago block is prone to deformation due to contrasts in crustal properties compared to the surrounding stronger blocks such as Maitai, Median Batholith, and central Canterbury (Gerbault et al., 2003; Upton et al.,

2014). Strain induced by the oblique plate convergence since Miocene results in roughly E-W contractions within the broadly deformed Otago block (Beavan et al., 2007), as shown in Fig. 9c. Therefore, we suspect that the imposing strain on the weak Otago crust leads to the formation of N-S foliations or macrostructures in the schist domain, thereby causing significant anisotropy with N-S oriented FVDs. The interpretation is further supported by the northward trend of mesoscopic folds and lineations in the central Otago schists (Wood, 1963), as well as laboratory measurements showing that anisotropy in the schist exhibits fast axes parallel to the foliation and lineation (Godfrey et al., 2000). Given the distribution of the schist, it is highly likely that the strong anisotropy is an intracrystalline feature extending southeastward, encompassing the entire Otago domain (Eberhart-Phillips et al., 2022; Reyners et al., 2017b). However, the limited resolution in the southeastern South Island impedes a comprehensive examination of its spatial extent and geometry in that region.

5.2.2. Northern South Island

The northern South Island represents a region where extensive crustal deformation occurs due to transition in tectonic regime from oblique convergence to transpression (Fig. 1). Previous studies on local shear wave splitting suggest that crustal anisotropy beneath the Marlborough Fault System (MFS) is primarily controlled by structures, showing fast axes parallel to the fault strands (Audoine et al., 2000; Balfour et al., 2005). These observations are consistent with the NE-SW FVDs identified in our model at shallow depths (Fig. 8a), which could be attributed to shearing-induced fracturing along a series of subparallel faults in the MFS.

In the middle to lower crust, increasing confining pressure results in pervasive closures of microcracks, which explains the deviation of FVDs from the fault strike. At these depths, our model demonstrates a sharp change in anisotropy across the MFS (Fig. 8b–g), showing large and consistent NW-SE FVDs in the southeast and NE-SW FVDs to the northwest (Fig. 8b–g). This pattern aligns well with the shear wave splitting results of Graham et al. (2020) (Fig. S11), who suggest that topography-induced gravitational stress could be the main driver for the NW-SE FVDs. While this interpretation is plausible, it is difficult to reconcile the observed change in fast orientation and the reduction in anisotropy strength at shallower depths in our model. On the other hand, Eberhart-Phillips and Mark Henderson (2004) suggest that ductile deformation in the middle/lower crust due to plate convergence contributes to the plate motion aligned FVDs southeast of MFS. However, the interpretation may face some challenges considering that nearly all of the relative plate motions in the northern South Island are accommodated by shearing in the upper plate (Wallace et al., 2012a), posing a conflict with the observed high anisotropy along the subduction thrust. Moreover, we find that the trench-perpendicular FVDs in our model extend further south to regions north of Christchurch, surpassing the mapped Hikurangi Trough (Fig. 8d–g). This intriguing feature may suggest an alternative cause for the observed anisotropy.

It is now well acknowledged that the Hikurangi Plateau has experienced two episodes of subduction (e.g., Eberhart-Phillips et al., 2022; Reyners et al., 2011, 2017b). Unlike the present-day westward subduction beneath the Australian Plate, the initial phase of the southward subduction along the Gondwana margin at ~100 Ma resulted in a significant portion of the plateau being subducted and underplated beneath the Chatham Rise and much of South Island (Fig. 2b; Davy et al., 2008; Eberhart-Phillips et al., 2022; Reyners et al., 2017b). Previous tomographic studies have delineated the top of the underplated plateau to lie at 10–30 km along the eastern coast of the northern South Island, gradually shallowing towards the south to the region near Christchurch (e.g., Reyners et al., 2017a). These depths agree with the depths of the observed strong anisotropy in our model (Fig. 8d–g). Therefore, we speculate that deformation associated with paleostain accumulation along the Cretaceous subduction channel may be responsible for the strong anisotropy with NW-SE FVDs in the northern South Island. It is

even possible that the strong anisotropy reflects frozen-in fabrics during the formation of the oceanic plateau (Stern et al., 2020). Notably, paleostrain-induced anisotropy has been identified in the upper crust near Christchurch, reflecting inherited crustal weakness that played a role in the 2011 Canterbury earthquake (Fry et al., 2014). Similar scenarios have been observed in southern California, where paleofabrics related to the long-lived Mesozoic subduction have not been overprinted by the current transform motion (Schulte-Pelkum et al., 2021; Wu et al., 2022). In this context, the sudden change of FVDs north of Christchurch might correspond to the southern boundary of the underplated plateau or reflect a step of the slab that deepens further south. The latter case is more plausible since fast P-wave precursors generated by the high-velocity Hikurangi Plateau are observed south of Christchurch (Love et al., 2015). However, we reiterate that the limitations in model resolution prohibit us to trace the underplated Hikurangi Plateau further south and at greater depths beneath the central South Island.

6. Conclusions

We present a New Zealand-wide azimuthal anisotropic model using over 1 million local first P-wave arrival times and a recently developed adjoint-state traveltimes tomography method. The model is built on top of the New Zealand-wide isotropic model, and extends to a depth of 40 km. The key discoveries from this study are summarized below.

Our model reveals significant anisotropy variations in the North Island of New Zealand, showing distinct fast velocity directions (FVDs) between the Hikurangi forearc and backarc. Beneath the forearc, notable along-strike transitions of anisotropies are seen in the crust. At shallow depths (< 8 km), FVDs shift from trench-parallel (NE-SW) in the north to plate motion aligned (E-W) in the south, reflecting changes of tectonic stress and thus deformation regime in the upper plate as a result of the forearc rotation. At greater depths approaching the slab interface, north-south differences in anisotropy persist in the forearc but with distinct FVDs compared to the upper crust, showing trench-perpendicular directions in the north and trench-parallel directions in the south. The north-south transition boundary precisely matches the change in interplate coupling along the subduction megathrust. Thus, we ascribe the along-strike changes in anisotropy at greater depths to different deformation states related to the megathrust slip behaviors. The two-layered anisotropy may suggest a stress layering beneath the Hikurangi forearc, in agreement with stress measurements in previous studies. Beneath the backarc, we ascribe the N-S FVDs in regions with low strain rates to structural/rock fabrics. On the other hand, the strong anisotropy in the middle to lower crust beneath the southern backarc may stem from pure shear deformation in response to the change in backarc deformation from extension to compression from north to south.

Beneath the South Island, our model shows more homogenous anisotropy variations compared to the North Island. In the central South Island, anisotropies with increasing amplitude toward the Otago domain are interpreted as mineral-induced anisotropy within the Haast schist. We suggest that the roughly N-S fast directions in the schist domain are caused by the foliations formed by the oblique plate convergence. In the northern South Island, except the shallow anisotropies that are controlled by extensive faulting, the anisotropy at greater depths may relate to paleostrain during Cretaceous subduction along the Gondwana margin. The spatial extent of anisotropy with NW-SE FVDs may further delineate the subducted and underplated Hikurangi Plateau beneath the South Island.

CRediT authorship contribution statement

Shucheng Wu: Writing – review & editing, Writing – original draft, Investigation, Formal analysis, Conceptualization. **Jing Chen:** Writing – review & editing, Validation. **Ping Tong:** Writing – review & editing, Supervision, Software, Methodology, Conceptualization.

Declaration of competing interest

The authors declare that they have no known competing financial interests or personal relationships that could have appeared to influence the work reported in this paper.

Acknowledgements

This work was funded by Singapore Ministry of Education (MOE) Academic Research Fund (AcRF) Tier 2 Grant (MOE-T2EP20122-0008) and the National Science Foundation of China (grant 42474073). TP was also supported by MOE AcRF Tier 1 Grant (RT12/22). WSC was partially supported by MOST Special Fund from State Key Laboratory of Geological Processes and Mineral Resources, China University of Geosciences (grants MSFGPMR2022-6 and MSFGPMR2024-604). We sincerely thank Dr. Finnigan Illsley-Kemp, Prof. Martha Savage, and an anonymous reviewer for their insightful comments and constructive suggestions, which have greatly improved the quality of this manuscript. Figures in this paper were generated by Generic Mapping Tools (Wessel et al., 2013). Traveltimes data used in this study are archived in the ISC Bulletin (<https://doi.org/10.31905/D808B830>). The final model and relocated catalog can be accessed via <https://doi.org/10.21979/N9/QKU80S>.

Supplementary materials

Supplementary material associated with this article can be found, in the online version, at [doi:10.1016/j.epsl.2025.119362](https://doi.org/10.1016/j.epsl.2025.119362).

Data availability

All the traveltimes data used in this work are publicly available from the cited data sources. The results of this work including the velocity model and relocated earthquake catalog can be accessed via <https://doi.org/10.21979/N9/QKU80S>.

References

- Audet, P., 2015. Layered crustal anisotropy around the San Andreas Fault near Parkfield, California. *J. Geophys. Res.: Solid Earth* 120 (5), 3527–3543. <https://doi.org/10.1002/2014jb011821>.
- Audoine, E., Savage, M.K., Gledhill, K., 2000. Seismic anisotropy from local earthquakes in the transition region from a subduction to a strike-slip plate boundary, New Zealand. *J. Geophys. Res.: Solid Earth* 105 (B4), 8013–8033. <https://doi.org/10.1029/1999jb900444>.
- Audoine, E., Savage, M.K., Gledhill, K., 2004. Anisotropic structure under a back arc spreading region, the Taupo Volcanic Zone, New Zealand. *J. Geophys. Res.: Solid Earth* 109 (B11). <https://doi.org/10.1029/2003jb002932>.
- Balfour, N.J., Savage, M.K., Townsend, J., 2005. Stress and crustal anisotropy in Marlborough, New Zealand: evidence for low fault strength and structure-controlled anisotropy. *Geophys. J. Int.* 163 (3), 1073–1086. <https://doi.org/10.1111/j.1365-246X.2005.02783.x>.
- Bannister, S., Bryan, C.J., Bibby, H.M., 2004. Shear wave velocity variation across the Taupo Volcanic Zone, New Zealand, from receiver function inversion. *Geophys. J. Int.* 159 (1), 291–310. <https://doi.org/10.1111/j.1365-246X.2004.02384.x>.
- Barnes, P.M., de Lépinay, B.M., Collot, J.Y., Delteil, J., Audru, J.C., 1998. Strain partitioning in the transition area between oblique subduction and continental collision, Hikurangi margin, New Zealand. *Tectonics* 17 (4), 534–557. <https://doi.org/10.1029/98tc00974>.
- Bassett, D., Fujie, G., Kodaira, S., Arai, R., Yamamoto, Y., Henrys, S., Mochizuki, K., 2023. Heterogeneous crustal structure of the Hikurangi Plateau revealed by SHIRE seismic data: origin and implications for plate boundary tectonics. *Geophys. Res. Lett.* (22), 50. <https://doi.org/10.1029/2023gl105674>.
- Bassett, D., Sutherland, R., Henrys, S., 2014. Slow wavespeeds and fluid overpressure in a region of shallow geodetic locking and slow slip, Hikurangi subduction margin, New Zealand. *Earth Planet Sci. Lett.* 389, 1–13. <https://doi.org/10.1016/j.epsl.2013.12.021>.
- Beavan, J., Ellis, S., Wallace, L., Denys, P., 2007. Kinematic Constraints from GPS on Oblique Convergence of the Pacific and Australian Plates, Central South Island, New Zealand. A Continental Plate Boundary: Tectonics at South Island, New Zealand, pp. 75–94.
- Beavan, J., Wallace, L.M., Palmer, N., Denys, P., Ellis, S., Fournier, N., Denham, M., 2016. New Zealand GPS velocity field: 1995–2013. *New Zealand J. Geol. Geophys.* 59 (1), 5–14. <https://doi.org/10.1080/00288306.2015.1112817>.

- Behboudi, E., McNamara, D.D., Lokmer, I., Wallace, L.M., Saffer, D.M., 2022. Spatial variation of shallow stress orientation along the Hikurangi subduction margin: insights from In-situ borehole image logging. *J. Geophys. Res.: Solid Earth* 127 (5). <https://doi.org/10.1029/2021jb023641>.
- Benson, A.M., Little, T.A., Van Dissen, R.J., Hill, N., Townsend, D.B., 2001. Late quaternary paleoseismic history and surface rupture characteristics of the eastern Awatere strike-slip fault, New Zealand. *GSA Bulletin* 113 (8), 1079–1091. [https://doi.org/10.1130/0016-7606\(2001\)113-1079:LQPHAS>2.0.CO;2](https://doi.org/10.1130/0016-7606(2001)113-1079:LQPHAS>2.0.CO;2).
- Bibby, H.M., Caldwell, T.G., Davey, F.J., Webb, T.H., 1995. Geophysical evidence on the structure of the Taupo Volcanic Zone and its hydrothermal circulation. *J. Volcanol. Geotherm. Res.* 68 (1–3), 29–58. [https://doi.org/10.1016/0377-0273\(95\)00007-h](https://doi.org/10.1016/0377-0273(95)00007-h).
- Boness, N.L., Zoback, M.D., 2004. Stress-induced seismic velocity anisotropy and physical properties in the SAFOD Pilot Hole in Parkfield, CA. *Geophys. Res. Lett.* 31 (15). <https://doi.org/10.1029/2003gl019020>. L15S17.
- Boness, N.L., Zoback, M.D., 2006. Mapping stress and structurally controlled crustal shear velocity anisotropy in California. *Geology* (10), 34. <https://doi.org/10.1130/g22309.1>.
- Chow, B., Kaneko, Y., Tape, C., Modrak, R., Mortimer, N., Bannister, S., Townend, J., 2022. Strong upper-plate heterogeneity at the Hikurangi subduction margin (North Island, New Zealand) imaged by adjoint tomography. *J. Geophys. Res.: Solid Earth* 127 (1). <https://doi.org/10.1029/2021jb022865>.
- Crampin, S., 1987. Geological and industrial implications of extensive-dilatancy anisotropy. *Nature* 328 (6130), 491–496. <https://doi.org/10.1038/328491a0>.
- Crampin, S., 1991. Wave propagation through fluid-filled inclusions of various shapes: interpretation of extensive-dilatancy anisotropy. *Geophys. J. Int.* 104 (3), 611–623. <https://doi.org/10.1111/j.1365-246X.1991.tb05705.x>.
- Davy, B., Hoernle, K., Werner, R., 2008. Hikurangi Plateau: crustal structure, rifted formation, and Gondwana subduction history. *Geochem., Geophys., Geosyst.* 9 (7). <https://doi.org/10.1029/2007gc001855> n/a-n/a.
- Eberhart-Phillips, D., Bannister, S., Reyners, M., 2017. Deciphering the 3-D distribution of fluid along the shallow Hikurangi subduction zone using P- and S-wave attenuation. *Geophys. J. Int.* 211 (2), 1032–1045. <https://doi.org/10.1093/gji/ggx348>.
- Eberhart-Phillips, D., Mark Henderson, C., 2004. Including anisotropy in 3-D velocity inversion and application to Marlborough, New Zealand. *Geophys. J. Int.* 156 (2), 237–254. <https://doi.org/10.1111/j.1365-246X.2003.02044.x>.
- Eberhart-Phillips, D., Reyners, M., 2009. Three-dimensional distribution of seismic anisotropy in the Hikurangi subduction zone beneath the central North Island, New Zealand. *J. Geophys. Res.* 114 (B6). <https://doi.org/10.1029/2008jb005947>.
- Eberhart-Phillips, D., Reyners, M., 2012. Imaging the Hikurangi Plate interface region, with improved local-earthquake tomography. *Geophys. J. Int.* 190 (2), 1221–1242. <https://doi.org/10.1111/j.1365-246X.2012.05553.x>.
- Eberhart-Phillips, D., Reyners, M., Bannister, S., Chadwick, M., Ellis, S., 2010. Establishing a versatile 3-D seismic velocity model for New Zealand. *Seismolog. Res. Lett.* 81 (6), 992–1000. <https://doi.org/10.1785/gssrl.81.6.992>.
- Eberhart-Phillips, D., Reyners, M., Chadwick, M., Stuart, G., 2008. Three-dimensional attenuation structure of the Hikurangi subduction zone in the central North Island, New Zealand. *Geophys. J. Int.* 174 (1), 418–434. <https://doi.org/10.1111/j.1365-246X.2008.03816.x>.
- Eberhart-Phillips, D., Upton, P., Reyners, M., Barrell, D.J.A., Fry, B., Bourguignon, S., Warren-Smith, E., 2022. The influence of basement terranes on tectonic deformation: joint earthquake travel-time and ambient noise tomography of the Southern South Island, New Zealand. *Tectonics* 41. <https://doi.org/10.1029/2021tc007006>.
- Evanzia, D., Wilson, T., Savage, M.K., Lamb, S., Hirschberg, H., 2017. Stress orientations in a locked subduction zone at the southern Hikurangi Margin, New Zealand. *J. Geophys. Res.: Solid Earth* 122 (10), 7895–7911. <https://doi.org/10.1002/2017jb013998>.
- Fagereng, A., Ellis, S., 2009. On factors controlling the depth of interseismic coupling on the Hikurangi subduction interface, New Zealand. *Earth Planet Sci. Lett.* 278 (1–2), 120–130. <https://doi.org/10.1016/j.epsl.2008.11.033>.
- Fry, B., Davey, F., Eberhart-Phillips, D., Lebedev, S., 2014. Depth variable crustal anisotropy, patterns of crustal weakness, and destructive earthquakes in Canterbury, New Zealand. *Earth Planet Sci. Lett.* 392, 50–57. <https://doi.org/10.1016/j.epsl.2014.02.013>.
- Gerbault, M., Henrys, S., Davey, F., 2003. Numerical models of lithospheric deformation forming the Southern Alps of New Zealand. *J. Geophys. Res.: Solid Earth* 108 (B7). <https://doi.org/10.1029/2001jb001716>.
- Godfrey, N.J., Christensen, N.I., Okaya, D.A., 2000. Anisotropy of schists: contribution of crustal anisotropy to active source seismic experiments and shear wave splitting observations. *J. Geophys. Res.: Solid Earth* 105 (B12), 27991–28007. <https://doi.org/10.1029/2000jb000286>.
- Gou, T., Zhao, D., Huang, Z., Wang, L., 2018. Anisotropic 3-D ray tracing and its application to Japan Subduction Zone. *J. Geophys. Res.: Solid Earth* 123 (5), 4088–4108. <https://doi.org/10.1029/2017jb015321>.
- Graham, K.M., Savage, M.K., Arnold, R., Zal, H.J., Okada, T., Iio, Y., Matsumoto, S., 2020. Spatio-temporal analysis of seismic anisotropy associated with the Cook Strait and Kaikoura earthquake sequences in New Zealand. *Geophys. J. Int.* 223 (3), 1987–2008. <https://doi.org/10.1093/gji/ggaa433>.
- Heise, W., Bibby, H.M., Caldwell, T.G., Bannister, S.C., Ogawa, Y., Takakura, S., Uchida, T., 2007. Melt Distribution Beneath a Young Continental Rift: The Taupo Volcanic Zone. *Geophysical Research Letters*, New Zealand, p. 34. <https://doi.org/10.1029/2007gl029629>.
- Huang, Z., Tilmann, F., Comte, D., Zhao, D., 2019. P wave azimuthal anisotropic tomography in Northern Chile: insight into deformation in the subduction zone. *J. Geophys. Res.: Solid Earth* 124 (1), 742–765. <https://doi.org/10.1029/2018jb016389>.
- Huang, Z., Zhao, D., 2021. Mantle Convection in Subduction Zones. *Mantle Convection and Surface Expressions*, pp. 283–301.
- Huang, Z., Zhao, D., Liu, X., 2015. On the trade-off between seismic anisotropy and heterogeneity: numerical simulations and application to Northeast Japan. *J. Geophys. Res.: Solid Earth* 120 (5), 3255–3277. <https://doi.org/10.1002/2014jb011784>.
- Illsley-Kemp, F., Savage, M.K., Wilson, C.J.N., Bannister, S., 2019. Mapping stress and structure from subducting slab to magmatic rift: crustal seismic anisotropy of the North Island, New Zealand. *Geochem., Geophys., Geosyst.* 20 (11), 5038–5056. <https://doi.org/10.1029/2019gc008529>.
- ISC. (2022). International Seismological Centre on-line Bulletin. [doi:10.31905/D808B830](https://doi.org/10.31905/D808B830).
- Johnson, J.H., Savage, M.K., Townend, J., 2011. Distinguishing between stress-induced and structural anisotropy at Mount Ruapehu volcano, New Zealand. *J. Geophys. Res.* 116 (B12). <https://doi.org/10.1029/2011jb008308>.
- Karalliyadda, S.C., Savage, M.K., 2013. Seismic anisotropy and lithospheric deformation of the plate-boundary zone in South Island, New Zealand: inferences from local S-wave splitting. *Geophys. J. Int.* 193 (2), 507–530. <https://doi.org/10.1093/gji/ggt022>.
- Kreemer, C., Blewitt, G., Klein, E.C., 2014. A geodetic plate motion and global strain rate model. *Geochem., Geophys., Geosyst.* 15 (10), 3849–3889. <https://doi.org/10.1002/2014gc005407>.
- Langridge, R.M., Berryman, K.R., 2005. Morphology and slip rate of the Hurunui section of the Hope Fault, South Island, New Zealand. *New Zealand J. Geol. Geophys.* 48 (1), 43–57. <https://doi.org/10.1080/00288306.2005.9515097>.
- Little, T.A., Mortimer, N., McWilliams, M., 1999. An episodic cretaceous cooling model for the Otago-Marlborough Schist, New Zealand, based on 40Ar/39Ar white mica ages. *New Zealand J. Geol. Geophys.* 42 (3), 305–325. <https://doi.org/10.1080/00288306.1999.9514848>.
- Liu, X., Zhao, D., 2017. Depth-varying azimuthal anisotropy in the Tohoku subduction channel. *Earth Planet Sci. Lett.* 473, 33–43. <https://doi.org/10.1016/j.epsl.2017.05.034>.
- Love, H., LeGood, M., Stuart, G., Reyners, M., Eberhart-Phillips, D.E., Gubbins, D., 2015. Fast P-wave precursors in New Zealand: high velocity material associated with the subducted Hikurangi Plateau. *Geophys. J. Int.* 202 (2), 1223–1240. <https://doi.org/10.1093/gji/ggv205>.
- Mason, D.P.M., Little, T.A., Van Dissen, R.J., 2006. Rates of active faulting during late quaternary fluvial terrace formation at Saxton River, Awatere fault, New Zealand. *GSA Bulletin* 118 (11–12), 1431–1446. <https://doi.org/10.1130/B25961.1>.
- Morley, A.M., Stuart, G.W., Kendall, J.M., Reyners, M., 2006. Mantle wedge anisotropy in the Hikurangi subduction zone, central North Island, New Zealand. *Geophys. Res. Lett.* 33. <https://doi.org/10.1029/2005gl024569>.
- Mortimer, N., 2004. New Zealand's geological foundations. *Gondwana Res.* 7 (1), 261–272. [https://doi.org/10.1016/s1342-937x\(05\)70324-5](https://doi.org/10.1016/s1342-937x(05)70324-5).
- Nicol, A., Mazengarb, C., Chanier, F., Rait, G., Uruski, C., Wallace, L., 2007. Tectonic evolution of the active Hikurangi subduction margin, New Zealand, since the Oligocene. *Tectonics* 26 (4), TC4002. <https://doi.org/10.1029/2006tc002090>.
- Reyners, M., 2013. The central role of the Hikurangi Plateau in the cenozoic tectonics of New Zealand and the Southwest Pacific. *Earth Planet Sci. Lett.* 361, 460–468. <https://doi.org/10.1016/j.epsl.2012.11.010>.
- Reyners, M., Eberhart-Phillips, D., Bannister, S., 2011. Tracking repeated subduction of the Hikurangi Plateau beneath New Zealand. *Earth Planet Sci. Lett.* 311 (1–2), 165–171. <https://doi.org/10.1016/j.epsl.2011.09.011>.
- Reyners, M., Eberhart-Phillips, D., Bannister, S., 2017a. Subducting an old subduction zone sideways provides insights into what controls plate coupling. *Earth Planet Sci. Lett.* 466, 53–61. <https://doi.org/10.1016/j.epsl.2017.03.004>.
- Reyners, M., Eberhart-Phillips, D., Upton, P., Gubbins, D., 2017b. Three-dimensional imaging of impact of a large igneous province with a subduction zone. *Earth Planet Sci. Lett.* 460, 143–151. <https://doi.org/10.1016/j.epsl.2016.12.025>.
- Salmon, M., Kennett, B.L.N., Stern, T., Aitken, A.R.A., 2013. The Moho in Australia and New Zealand. *Tectonophysics* 609, 288–298. <https://doi.org/10.1016/j.tecto.2012.07.009>.
- Salmon, M.L., Stern, T.A., Savage, M.K., 2011. A major step in the continental Moho and its geodynamic consequences: the Taranaki-Ruapehu line, New Zealand. *Geophys. J. Int.* 186 (1), 32–44. <https://doi.org/10.1111/j.1365-246X.2011.05035.x>.
- Schulte-Pelkum, V., Becker, T.W., Behr, W.M., Miller, M.S., 2021. Tectonic inheritance during plate boundary evolution in Southern California constrained from seismic anisotropy. *Geochem., Geophys., Geosyst.* 22, 22. <https://doi.org/10.1029/2021gc010099>.
- Stern, T., Benson, A., 2011. Wide-angle seismic imaging beneath an andesitic arc: central North Island, New Zealand. *J. Geophys. Res.* 116 (B9). <https://doi.org/10.1029/2011jb008337>.
- Stern, T., Lamb, S., Moore, J.D.P., Okaya, D., Hochmuth, K., 2020. High mantle seismic P-wave speeds as a signature for gravitational spreading of superplumes. *Sci. Adv.* 6 (22), eaba7118. <https://doi.org/10.1126/sciadv.aba7118>.
- Stern, T.A., Stratford, W.R., Salmon, M.L., 2006. Subduction evolution and mantle dynamics at a continental margin: central North Island, New Zealand. *Rev. Geophys.* 44 (4), RG4002. <https://doi.org/10.1029/2005rg000171>.
- Tong, P., 2021. Adjoint-State traveltome tomography for azimuthally anisotropic Media and insight into the crustal structure of Central California near Parkfield. *J. Geophys. Res.: Solid Earth* 126 (10), e2021JB022365. <https://doi.org/10.1029/2021jb022365>.

- Tong, P., Li, T., Chen, J., Nagaso, M., 2024. Adjoint-state differential arrival time tomography. *Geophys. J. Int.* 236 (1), 139–160. <https://doi.org/10.1093/gji/ggad416>.
- Townend, J., Sherburn, S., Arnold, R., Boese, C., Woods, L., 2012. Three-dimensional variations in present-day tectonic stress along the Australia–Pacific plate boundary in New Zealand. *Earth Planet Sci. Lett.* 353–354, 47–59. <https://doi.org/10.1016/j.epsl.2012.08.003>.
- Upton, P., Craw, D., Walcott, R., 2014. Far-field deformation resulting from rheologic differences interacting with tectonic stresses: an example from the Pacific/Australian plate boundary in southern New Zealand. *Geosciences (Basel)* 4 (3), 93–113. <https://doi.org/10.3390/geosciences4030093>.
- Wallace, L.M., Barnes, P., Beavan, J., Van Dissen, R., Litchfield, N., Mountjoy, J., Pondard, N., 2012a. The kinematics of a transition from subduction to strike-slip: an example from the central New Zealand plate boundary. *J. Geophys. Res.: Solid Earth* 117 (B2), B02405. <https://doi.org/10.1029/2011jb008640>.
- Wallace, L.M., Beavan, J., Bannister, S., Williams, C., 2012b. Simultaneous long-term and short-term slow slip events at the Hikurangi subduction margin, New Zealand: implications for processes that control slow slip event occurrence, duration, and migration. *J. Geophys. Res.: Solid Earth* 117 (B11), B11402. <https://doi.org/10.1029/2012jb009489>.
- Wallace, L.M., Beavan, J., McCaffrey, R., Darby, D., 2004. Subduction zone coupling and tectonic block rotations in the North Island, New Zealand. *J. Geophys. Res.: Solid Earth* 109 (B12). <https://doi.org/10.1029/2004jb003241>.
- Wallace, L.M., Fagereng, A., Ellis, S., 2012c. Upper plate tectonic stress state may influence interseismic coupling on subduction megathrusts. *Geology* 40 (10), 895–898. <https://doi.org/10.1130/g33373.1>.
- Wang, Y., 2014. Seismic ray tracing in anisotropic media: a modified Newton algorithm for solving highly nonlinear systems. *Geophysics* 79 (1), T1–T7. <https://doi.org/10.1190/geo2013-0110.1>.
- Warren-Smith, E., Lamb, S., Stern, T.A., Smith, E., 2017. Microseismicity in Southern South Island, New Zealand: implications for the mechanism of crustal deformation adjacent to a major continental transform. *J. Geophys. Res.: Solid Earth* 122 (11), 9208–9227. <https://doi.org/10.1002/2017jb014732>.
- Wessel, P., Smith, W.H.F., Scharroo, R., Luis, J., Wobbe, F., 2013. Generic mapping tools: improved version released. *Eos, Trans. Am. Geophys. Union* 94 (45), 409–410. <https://doi.org/10.1002/2013eo450001>.
- Williams, C.A., Eberhart-Phillips, D., Bannister, S., Barker, D.H.N., Henrys, S., Reyners, M., Sutherland, R., 2013. Revised interface geometry for the Hikurangi Subduction Zone, New Zealand. *Seismolog. Res. Lett.* 84 (6), 1066–1073. <https://doi.org/10.1785/0220130035>.
- Wood, B.L., 1963. Structure of the Otago schists. *New Zealand J. Geol. Geophys.* 6 (5), 641–680. <https://doi.org/10.1080/00288306.1963.10423606>.
- Wu, S., Jiang, C., Schulte-Pelkum, V., Tong, P., 2022. Complex patterns of past and ongoing crustal deformations in Southern California revealed by seismic azimuthal anisotropy. *Geophys. Res. Lett.* 49 (15). <https://doi.org/10.1029/2022gl100233> e2022GL100233.
- Zal, H.J., Jacobs, K., Savage, M.K., Yarce, J., Mroczeck, S., Graham, K., Henrys, S., 2020. Temporal and spatial variations in seismic anisotropy and vp/vs ratios in a region of slow slip. *Earth Planet Sci. Lett.* 532, 115970. <https://doi.org/10.1016/j.epsl.2019.115970>.
- Zhao, D., Yu, S., Liu, X., 2016. Seismic anisotropy tomography: new insight into subduction dynamics. *Gondwana Res.* 33, 24–43. <https://doi.org/10.1016/j.gr.2015.05.008>.